INTERNATIONAL JOURNAL OF MULTIDISCIPLINARY RESEARCH AND ANALYSIS

ISSN(print): 2643-9840, ISSN(online): 2643-9875

Volume 09 Issue 07 July 2026

DOI: 10.47191/ijmra/v9-i7-40, Impact Factor: 8.685

Page No. 4547-4562

In Silico Screening of 10 Natural Compounds from Oroxylum indicum and Other Medicinal Plants against SARS-CoV-2 Mpro

Vo Van On[1], Nguyen Thi Lien Thuong[2]

[1,2]Institute of Pharmaceuticals and Health Foods, Thu Dau Mot University, Ho Chi Minh City, Vietnam

ABSTRACT: This study conducted structure-based virtual screening using AutoDock Vina to assess the inhibitory potential of ten natural compounds against the main protease (Mpro/3CLpro, PDB: 6LU7) of SARS-CoV-2. The study aimed to identify promising anti-SARS-CoV-2 candidates from *Oroxylum indicum* and other medicinal plants. Six compounds were sourced from *Oroxylum indicum*: Oroxin B, Quercetin, Quercitrin, Isoquercitrin, Rutin, and Baicalein; four additional compounds were sourced from other medicinal plants: Artemisinin (*Artemisia annua*), Naringenin (*Citrus spp.*), 6-Gingerol (*Zingiber officinale*), and Andrographolide (*Andrographis paniculata*). All ten compounds established stable interactions within the Mpro active site, with ΔG values ranging from −5.2 to −7.3 kcal/mol. Artemisinin demonstrated the highest binding affinity (−7.3 kcal/mol) and the highest Ligand Efficiency (LE = 0.365 kcal/mol/HA), surpassing Favipiravir and approaching Remdesivir in per-atom efficiency. Detailed PLIP v2.4.0 interaction analysis identified conserved key residues GLN110 (present in 9/10 complexes), THR111, VAL104, PHE294, LYS5, GLU288/290, and LYS137, with diverse interaction types including H-bonds (1–10 per complex), hydrophobic contacts, salt bridges, π-cation, and π-stacking interactions. Baicalein, Naringenin, Quercetin, and Artemisinin fully satisfied Lipinski and Veber criteria, predicting favorable oral bioavailability. These results provide a multi-level in silico evidence base supporting preclinical research on *Oroxylum indicum* constituents and Vietnamese medicinal plant-derived compounds as anti-SARS-CoV-2 candidates.

KEYWORDS: Molecular docking; SARS-CoV-2 Mpro; *Oroxylum indicum*; natural compounds; Baicalein; Artemisinin; Naringenin; PLIP; ADMET; COVID-19.

I. INTRODUCTION

The COVID-19 pandemic caused by SARS-CoV-2 has posed a severe global health challenge, driving an urgent need for novel antiviral agents [1,2]. The main protease Mpro (3CLpro) has been identified as an ideal pharmacological target owing to its indispensable role in viral replication and the absence of closely homologous proteins in humans [3]. Mpro is a cysteine protease that functions as a homodimer with a catalytic dyad Cys145–His41, cleaving the viral polyprotein at 11 conserved sites to generate essential non-structural proteins [4]. Its structure has been resolved at high resolution (PDB: 6LU7, 2.16 Å) [5], providing an excellent foundation for large-scale in silico screening.

Despite the rapid global rollout of vaccines, SARS-CoV-2 continues to evolve, with successive variants of concern eroding vaccine- and infection-induced immunity and sustaining transmission worldwide [6]. A substantial proportion of infected individuals also go on to develop long COVID, a debilitating multisystem condition with persistent symptoms that further exposes the limits of current preventive measures [7]. These ongoing challenges reinforce the need for effective, broadly active antiviral therapeutics targeting conserved viral machinery, such as Mpro.

Several Mpro-targeted antivirals have since reached clinical use, most notably the Pfizer oral inhibitor nirmatrelvir (marketed as Paxlovid), which demonstrated potent antiviral activity and a favorable safety profile in clinical trials [8]. However, real-world use of nirmatrelvir has been complicated by viral rebound after treatment, mandatory co-administration with the CYP3A4 inhibitor ritonavir (with attendant drug–drug interactions), restricted access in low- and middle-income countries, and the emergence of naturally occurring Mpro mutations conferring measurable in vitro resistance [9]. Because Mpro is highly conserved across coronavirus genera and has no human structural homolog, it remains an attractive target for novel chemical scaffolds that can complement or circumvent these limitations [10].

Plant-derived compounds have attracted considerable attention owing to their structural diversity, low toxicity, and long history of safe use in traditional medicine [11,12]. Phytochemicals from diverse taxa have demonstrated in vitro activity against multiple coronaviruses, including inhibition of viral entry, protease activity, and helicase function [13]. *Oroxylum indicum* (family Bignoniaceae) is widely used in Asian traditional medicine to treat respiratory inflammation and infections [14]. Its characteristic flavonoid constituents — baicalein, chrysin, oroxylin A, apigenin, quercetin, and their glycosides (oroxin A, oroxin B, quercitrin, isoquercitrin, rutin) — have been documented for a range of significant biological activities [14], most notably baicalein and its glycoside baicalin, whose anti-inflammatory, hepatoprotective, and antiviral pharmacology has been extensively reviewed [15]. Other Vietnamese medicinal plants, including ginger (*Zingiber officinale*), sweet wormwood (*Artemisia annua*) and king of bitters (*Andrographis paniculata*), also furnish bioactive compounds with diverse mechanisms of action.

Beyond *Oroxylum indicum*, each of the four additional compounds investigated here has independent experimental support for anti-SARS-CoV-2 potential. Artemisinin and related artemisinin-based antimalarials, long established as first-line antimalarial therapy, inhibit SARS-CoV-2 replication in vitro [16]. Naringenin, a citrus-derived flavanone, has been proposed to interfere with both viral entry via ACE2 and Mpro activity while also exerting anti-inflammatory effects relevant to COVID-19-associated cytokine release [17]. 6-Gingerol, the principal pungent constituent of *Zingiber officinale*, shows favorable in silico affinity for the SARS-CoV-2 spike protein and ACE2 receptor, providing part of the rationale for its inclusion here [18]. Andrographolide, the major diterpenoid of *Andrographis paniculata*, inhibits SARS-CoV-2 replication in human lung epithelial cells [19], complementing the clinical efficacy data discussed in Table VI.

Molecular docking plays a pivotal role in the rapid screening of natural compound libraries [20], offering a computationally efficient means of prioritizing candidates prior to costly experimental validation, despite well-recognized limitations in scoring-function accuracy and receptor flexibility [21]. When combined with detailed interaction analysis via PLIP (Protein–Ligand Interaction Profiler) [22] and drug-likeness/ADMET evaluation, this approach constitutes an efficient hierarchical screening workflow. The present study pursued three objectives: (1) to perform molecular docking of ten compounds against Mpro (PDB: 6LU7) using AutoDock Vina; (2) to conduct detailed protein–ligand interaction analysis using PLIP v2.4.0; and (3) to perform a comprehensive drug-likeness and ADMET evaluation.

II. MATERIALS AND METHODS

A. Protein and Ligand Preparation

The crystal structure of SARS-CoV-2 Mpro was retrieved from the Protein Data Bank (PDB ID: 6LU7, resolution 2.16 Å) [5]. The protein was prepared by removing water molecules, adding hydrogen atoms, and optimizing its geometry with Open Babel 3.1.1. Three-dimensional ligand structures were downloaded from PubChem in SDF format, energy-minimized with the MMFF94 force field, and converted to PDBQT format. Nirmatrelvir, Remdesivir, and Favipiravir were used as reference drugs.

B. Molecular Docking Simulation

Molecular docking was carried out using AutoDock Vina 1.1.2 [23]. A 25 × 25 × 25 Å grid box centered at (−10.73; 12.42; 68.82) Å encompassed the active site containing the catalytic dyad Cys145–His41. Exhaustiveness was set to 8, with a maximum of 9 binding modes. The lowest-energy pose was reported. Ligand efficiency (LE) was calculated as LE = |ΔG| / number of heavy atoms.

C. Protein–Ligand Interaction Analysis by PLIP

Detailed interaction analysis was performed using PLIP v2.4.0 (Protein–Ligand Interaction Profiler) [22], an automated tool that detects and classifies interaction types, including hydrogen bonds (H-bonds), hydrophobic contacts, salt bridges, π-cation interactions, π-stacking, and halogen bonds. Each H-bond is characterized by the H–A distance (Å) and D–H–A angle (°). An H-bond was considered reliable when the H–A distance was <3.5 Å and the D–H–A angle was >120°. The input complex was the lowest-energy docking pose (mode 1) from AutoDock Vina.

D. Drug-Likeness and ADMET Evaluation

Drug-likeness was assessed according to Lipinski's Rule of Five (MW ≤ 500, LogP ≤ 5, HBD ≤ 5, HBA ≤ 10) [24] and Veber's rules (TPSA ≤ 140 Å², RotB ≤ 10) [25]. ADMET profiles and physicochemical parameters were predicted using SwissADME (swissadme.ch) [26].

III. RESULTS

A. Chemical Characterization of Study Compounds

Table I presents the chemical identities of the ten study compounds, including common names, scientific names of the source plants, PubChem CIDs, and molecular formulas, to support structure retrieval, verification, and the interpretation of the results.

Table I. Chemical Characterization of the Ten Study Compounds

No.	Compound	Common Name	Scientific Name (Source)	PubChem CID	Formula
1	Artemisinin	Sweet wormwood extract	Artemisia annua L.	68827	$C_{15}H_{22}O_5$
2	Quercetin	Trumpet tree (O. indicum)	Oroxylum indicum (L.) Kurz	5280343	$C_{15}H_{10}O_7$
3	Naringenin	Orange/grapefruit	Citrus sinensis (L.) Osbeck	932	$C_{15}H_{12}O_5$
4	Oroxin B	Trumpet tree (O. indicum)	Oroxylum indicum (L.) Kurz	64982	$C_{21}H_{18}O_{11}$
5	Rutin	Trumpet tree/fish mint	O. indicum / Houttuynia cordata Thunb.	5280805	$C_{27}H_{30}O_{16}$
6	Baicalein	Trumpet tree/skullcap	Oroxylum indicum (L.) Kurz	5281605	$C_{15}H_{10}O_5$
7	Andrographolide	King of bitters	Andrographis paniculata (Burm.f.) Nees	5318517	$C_{20}H_{30}O_5$
8	Quercitrin	Trumpet tree (O. indicum)	Oroxylum indicum (L.) Kurz	5280459	$C_{21}H_{20}O_{11}$
9	Isoquercitrin	Trumpet tree (O. indicum)	Oroxylum indicum (L.) Kurz	5280804	$C_{21}H_{20}O_{12}$
10	6-Gingerol	Fresh ginger root	Zingiber officinale Roscoe	442793	$C_{17}H_{26}O_4$

Note: *Scientific names of source plants are italicized per international nomenclature. Full structural information (SMILES, InChI) for each compound is available at pubchem.ncbi.nlm.nih.gov.*

Beyond the ligand series characterized above, Figure 1 shows the crystal structure of the docking receptor — the SARS-CoV-2 main protease (Mpro/3CLpro, PDB ID: 6LU7) — resolved at 2.16 Å resolution by X-ray crystallography [5]. The enzyme assembles as a homodimer (chain A and chain B), each protomer comprising two antiparallel β-barrel domains (I–II) that form the substrate-binding cleft harboring the catalytic dyad Cys145–His41, and a C-terminal α-helical domain (III) that mediates dimerization. Because an intact dimer interface is required for catalytic competence, the full biological assembly — rather than an isolated monomer — was used to define the docking grid in this study (Section II-A).

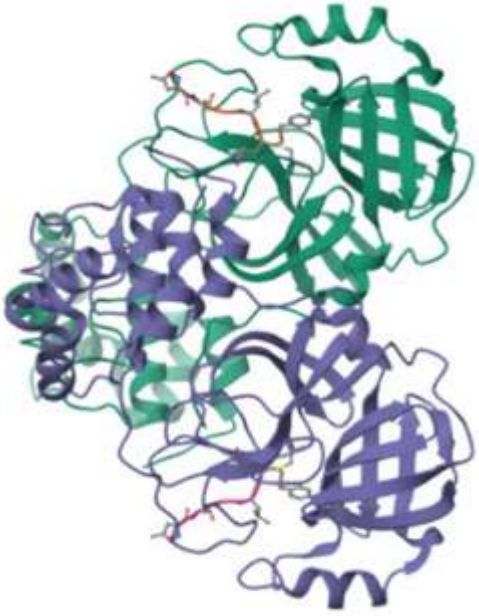

Figure 1. Crystal structure of the SARS-CoV-2 main protease (Mpro/3CLpro, PDB ID: 6LU7) resolved at 2.16 Å resolution [5], shown as the catalytically active homodimer (chain A, green; chain B, purple).

B. Molecular Docking Results

Table II presents the binding free energy (ΔG) and Ligand Efficiency (LE) of the ten compounds and three reference drugs against SARS-CoV-2 Mpro (PDB: 6LU7).

Table II. Binding Free Energy (ΔG) and Ligand Efficiency (LE) of Compounds against SARS-CoV-2 Mpro

No.	Compound	Source	ΔG (kcal/mol)	HA	LE	Rank
Ctrl1	Nirmatrelvir	Mpro inhibitor (FDA)	−9.15	23	0.398	—
Ctrl2	Remdesivir	Antiviral drug (FDA)	−8.15	36	0.226	—
1	Artemisinin	Artemisia annua	−7.3	20	0.365	1 ★
2	Quercetin	Oroxylum indicum	−6.9	22	0.314	2
3	Naringenin	Citrus spp.	−6.8	19	0.358	3
4	Oroxin B	Oroxylum indicum	−6.7	32	0.209	4
5	Rutin	O. indicum / H. cordata	−6.6	43	0.154	5
6	Baicalein	Oroxylum indicum	−6.6	20	0.330	6
7	Andrographolide	Andrographis paniculata	−6.0	25	0.240	7
8	Quercitrin	Oroxylum indicum	−5.6	32	0.175	8
9	Isoquercitrin	Oroxylum indicum	−5.4	33	0.164	9
10	6-Gingerol	Zingiber officinale	−5.2	21	0.248	10
Ctrl3	Favipiravir	Antiviral drug (PMDA)	−6.05	10	0.605	—

Note: HA = heavy atom count; LE = Ligand Efficiency = |ΔG|/HA; Ctrl = control. Ranking from 1 (highest affinity) to 10 (lowest).

Figure 2 visualizes and compares the binding free energy (|ΔG|) and Ligand Efficiency (LE) of the ten compounds with those of the three reference drugs (Nirmatrelvir, Remdesivir, and Favipiravir). Dashed lines correspond to the ΔG of each reference drug; red diamonds (♦) indicate LE values on the upper red axis.

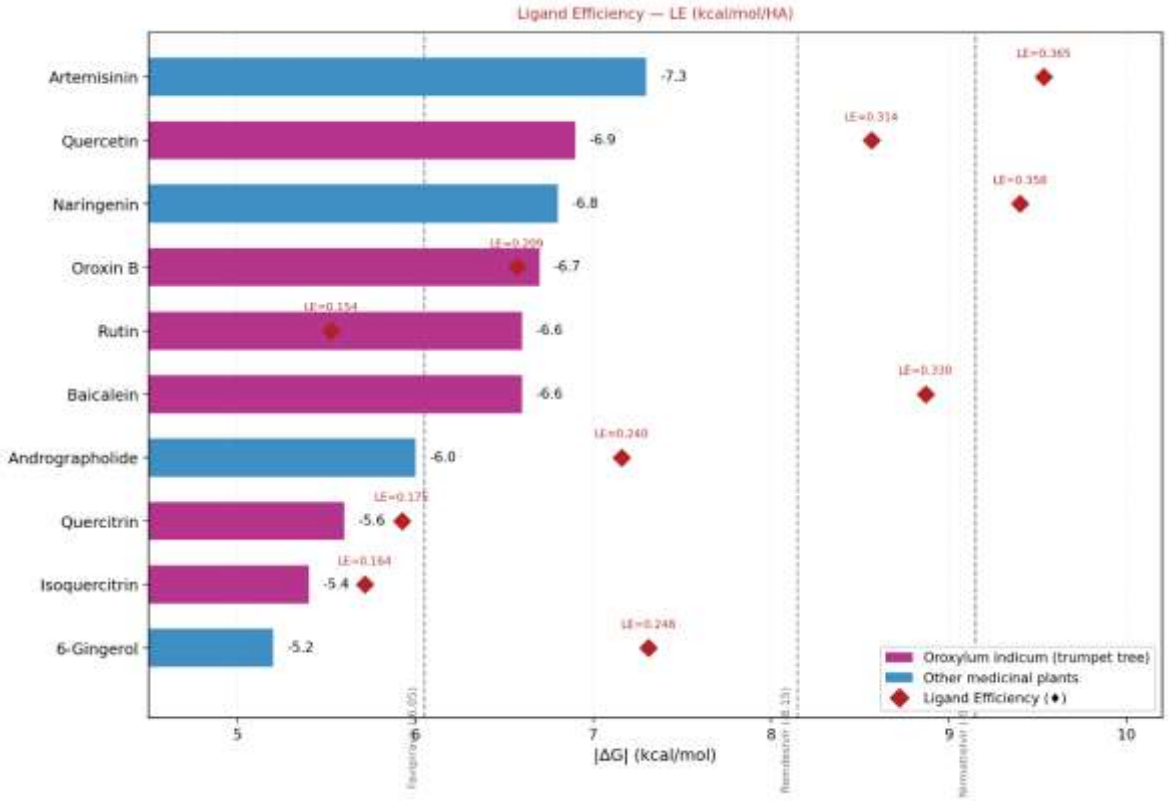

Figure 2. Comparison of binding free energy (ΔG, kcal/mol) and Ligand Efficiency (LE, kcal/mol/HA) for 10 natural compounds and reference drugs against SARS-CoV-2 Mpro (PDB: 6LU7).

Purple bars: compounds from Oroxylum indicum (trumpet tree); blue bars: other medicinal plants. Dashed lines: ΔG values of reference drugs. Red diamonds (◆): Ligand Efficiency (on the upper axis). Docking performed with AutoDock Vina 1.1.2, exhaustiveness = 8.

Ranked by binding affinity: artemisinin (−7.3) > quercetin (−6.9) > naringenin (−6.8) > oroxin B (−6.7) > rutin ≈ baicalein (−6.6) > andrographolide (−6.0) > quercitrin (−5.6) > isoquercitrin (−5.4) > 6-gingerol (−5.2) kcal/mol. This ranking is supported by PLIP analysis, which identified a diverse interaction network across the ten complexes. Artemisinin's LE of 0.365 kcal/mol/HA is the highest of the ten, reflecting efficient per-atom binding, and naringenin (0.358) and baicalein (0.330) are not far behind, marking all three as compact, efficient scaffolds. Seven of the ten compounds matched or exceeded favipiravir (−6.05 kcal/mol); only quercitrin, isoquercitrin, and 6-gingerol bound more weakly, and six of the ten surpassed the −6.5 kcal/mol mark.

C. PLIP Protein–Ligand Interaction Analysis

PLIP v2.4.0 analysis of all ten complexes identified a diverse interaction network comprising hydrogen bonds, hydrophobic contacts, salt bridges, π-cation, and π-stacking interactions, further detailing the binding patterns. Table III summarises the interaction profile of each complex.

Table III. Summary of Protein–Ligand Interaction Profiles Analyzed by PLIP v2.4.0

Compound	ΔG	H-bond	Hydro-phobic	Saltbridge	π-inter-action	Bidirec-tional	Total	Key Residues
Artemisinin	−7.3	1	5	0	None	0	6	GLN110, PHE294, ASN151, ILE106
Quercetin	−6.9	10	3	0	None	3 pairs	13	THR111, SER158, LYS102, GLN110
Naringenin	−6.8	5	5	0	None	0	10	PHE294★, THR111, GLN110, ASP295
Oroxin B	−6.7	3	4	3	None	1 pair	10	GLU288, GLU290, LYS5, ARG131, LYS137
Rutin	−6.6	7	1	3	None	2 pairs	11	LYS137★, GLU290, ASP289, LYS5
Baicalein	−6.6	5	4	0	None	1 pair	9	THR111 (×4)★, GLN110, VAL104
Andrographolide	−6.0	4	1	0	None	1 pair	5	VAL104★, ARG105 (bidirectional), GLN110
Quercitrin	−5.6	1	3	0	π-cation LYS5	0	5	LYS137, LYS5 (π-cation), TYR126
Isoquercitrin	−5.4	5	0	0	None	0	5	GLN127, THR169, LYS5, GLU288
6-Gingerol	−5.2	3	1	0	π-stack PHE294	0	5	PHE294 (π-stack P★), GLN110, SER158

★: record value in this series. π-interaction: π-cation or π-stacking.

Figure 3A presents a comprehensive PLIP interaction heatmap between the ten compounds and twelve key active-site residues of Mpro. This map enables rapid identification of conserved residues and cross-compound comparison of interaction depth.

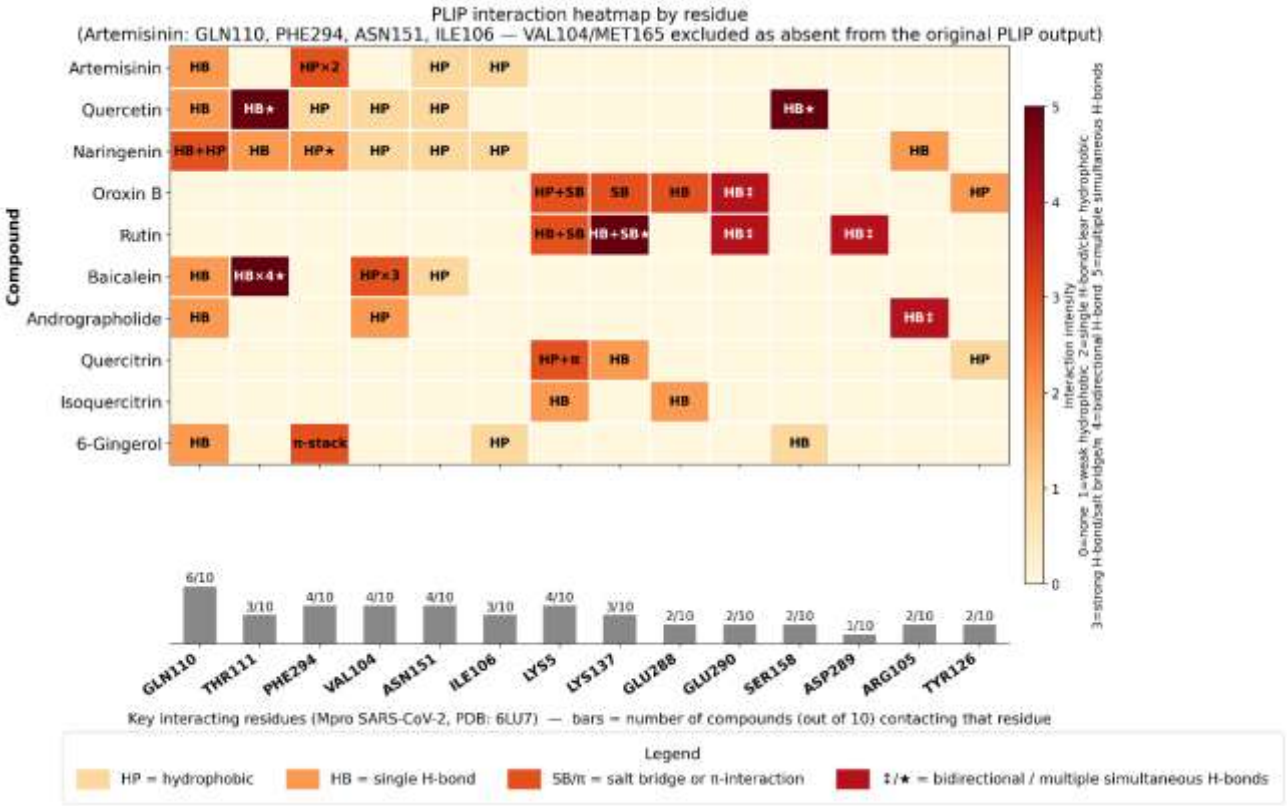

Figure 3A. PLIP interaction heatmap (Protein–Ligand Interaction Profiler v2.4.0) between the ten study compounds and key active-site residues of SARS-CoV-2 Mpro.

GLN110 is the most conserved residue (6/10 compounds). The color scale ranges from white (no interaction) to dark red (≥4 simultaneous/bidirectional H-bonds). Cell symbols: HP = hydrophobic; HB = H-bond; SB/π = salt bridge or π-interaction; ↕/★ = bidirectional or multiple simultaneous H-bonds. The bar row below the heatmap shows the number of compounds (out of 10) contacting each residue.

As a representative example of the residue-level interactions summarized in the heatmap above, Figure 3B shows the detailed two-dimensional PLIP interaction diagram [22] for the 6-Gingerol–Mpro complex (Section III-C-10). 6-Gingerol, the principal pungent constituent of *Zingiber officinale* [18], is highlighted here because it forms the most geometrically ideal π-stacking interaction observed in the entire series.

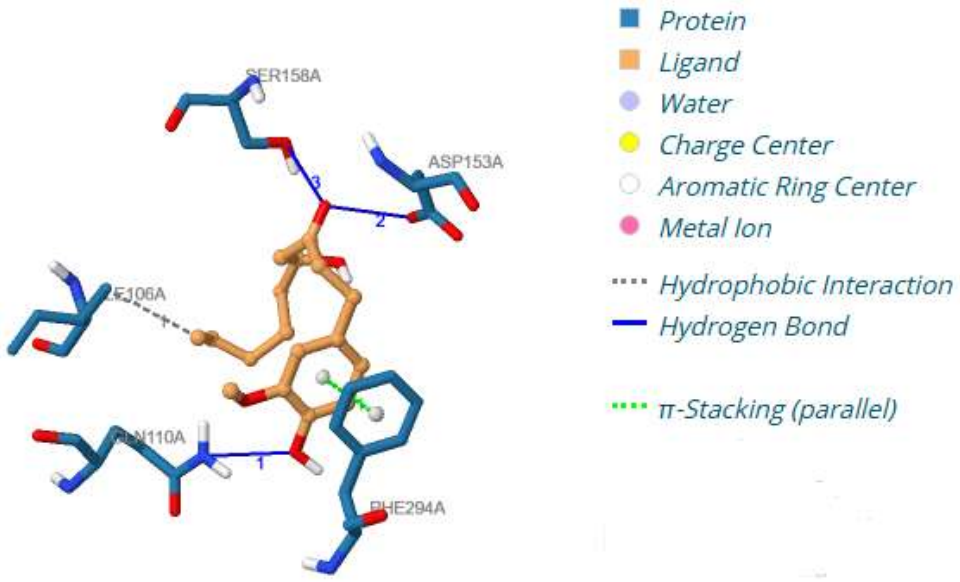

Figure 3B. Two-dimensional PLIP interaction diagram (chain A) for the 6-Gingerol–Mpro complex, generated with PLIP v2.4.0 [22].

1) *Artemisinin — ΔG = −7.3 kcal/mol, LE = 0.365: Artemisinin (sesquiterpene lactone from sweet wormwood, MW 282 Da) stands apart chemically from the other nine compounds: it has no aromatic ring, no H-bond donors, and zero rotatable bonds, making it essentially rigid. It also achieves the best docking score in the series (−7.3 kcal/mol) and the highest LE (0.365 kcal/HA). This is notable because it forms only one H-bond and five hydrophobic contacts, yet the single H-bond it does form, with GLN110, sits at 168.22°, the closest to the ideal 180° of any complex studied. PHE294 adds two further hydrophobic contacts (3.36 and 3.76 Å), with ASN151, ILE106, and ASP153 contributing additional hydrophobic contacts. The rigidity of the scaffold may help explain this result: without H-bond donors to rely on, artemisinin still binds tightest, possibly because its shape fits the pocket with minimal entropic penalty.*

2) *Quercetin — ΔG = −6.9 kcal/mol: Quercetin (flavone aglycone from O. indicum, MW 302 Da) forms 10 H-bonds across 6 distinct residues, the richest H-bond network in the series and unusually extensive for a molecule under 310 Da. The shortest of these, with SER158 (1.80 Å, 166.78°), is also the tightest SER158 contact seen anywhere in the series. THR111 acts as a hub, forming 3 simultaneous H-bonds (a 2.11 Å backbone contact plus a bidirectional sidechain pair at 2.50 Å and 2.68 Å), and three residue pairs overall (THR111, SER158, THR292) show bidirectional H-bonding, reflecting excellent geometric complementarity with the pocket. LYS102 contributes an electrostatic H-bond of 2.19 Å via its –NH_3^+ group, while ASP153 and GLN110 each add a further H-bond. In contrast to the preceding compound, three hydrophobic contacts round out the profile, with PHE294 (3.38 Å), ASN151, and VAL104. The resulting score of −6.9 kcal/mol is the best among all six O. indicum-derived compounds.*

3) *Naringenin — ΔG = −6.8 kcal/mol, LE = 0.358: Naringenin (a flavanone from Citrus spp., MW 254 Da) is the only flavanone among the ten compounds, and its non-planar C-ring (saturated at C2) confers a distinctive interaction profile. It reaches LE = 0.358, second only to artemisinin, with a well-balanced mix of 5 H-bonds and 5 hydrophobic contacts. The closest hydrophobic contact in the entire series is between PHE294 and 3.15 Å. A single hydroxyl group, the O3 hotspot, does much of the work, forming three H-bonds simultaneously with THR111 (2.17 Å), THR292 (3.27 Å), and ASP295 (2.39 Å), while GLN110 adds a well-geometried H-bond of its own (2.44 Å, 162.53°). Naringenin is also the first compound in the series to reach ARG105, forming a backbone H-bond at 2.54 Å, made possible by its non-planar C-ring protruding into the pocket. That same non-planarity opens access to regions (ARG105, PHE294) that the flatter, planar flavones in this set cannot reach, which likely explains why naringenin outperforms them in ligand efficiency despite a similar hydroxyl count.*

4) *Oroxin B — ΔG = −6.7 kcal/mol: Oroxin B (baicalein-7-O-β-D-glucuronide from O. indicum, MW 446 Da) relies heavily on its glucuronate carboxylate group, which forms three salt bridges, with LYS5 (5.42 Å), ARG131 (4.34 Å), and LYS137 (3.38 Å), that help anchor this comparatively large molecule in the pocket. Three H-bonds involve GLU288 (2.14 Å, 153.69°, the tightest H-bond angle in this complex) and a bidirectional pair with GLU290 (2.41 Å and 2.45 Å), while four hydrophobic contacts complete the picture, with LYS5 and TYR126 each contributing twice. This combination makes Oroxin B the only complex in the series to combine glucuronate-derived salt bridges with aglycone-derived H-bonds in the same binding mode.*

5) *Rutin — ΔG = −6.6 kcal/mol: Rutin (quercetin-3-O-rutinoside, MW 610 Da) is the largest molecule in the series (43 heavy atoms), yet it still manages a rich interaction profile of 7 H-bonds and 3 salt bridges. Its H-bond with LYS137 (1.92 Å, 165.92°) is the strongest of any complex studied, and ASP289 contributes two high-quality bidirectional H-bonds (backbone and sidechain). LYS5 simultaneously forms an H-bond (3.24 Å) and two salt bridges (5.22 Å and 5.19 Å), while GLU290 forms a further bidirectional H-bond pair. LEU286, a residue not observed elsewhere in the series, provides a unique hydrophobic contact, suggesting that rutin's di-glycoside chain allows it to reach a deeper hydrophobic region of the pocket than the other compounds do.*

6) *Baicalein — ΔG = −6.6 kcal/mol, LE = 0.330: Baicalein (5,6,7-trihydroxyflavone from O. indicum, MW 270 Da) reaches an LE of 0.330, the highest among O. indicum-derived compounds. THR111 alone accounts for 4 simultaneous H-bonds, the most seen at any single residue in the series: two short backbone contacts (1.98 Å and 2.00 Å) plus a bidirectional sidechain pair (3.12 Å and 3.26 Å). VAL104 adds 3 simultaneous hydrophobic contacts (3.62, 3.69, and 3.83 Å), consistent with how the flat, rigid flavone scaffold (only 1 rotatable bond) sits neatly against the VAL104 isopropyl group, and GLN110 contributes one further H-bond (2.56 Å). With this combination of high ligand efficiency and full compliance with drug-likeness rules, baicalein stands out as a leading scaffold among the O. indicum flavonoids.*

7) *Andrographolide — ΔG = −6.0 kcal/mol: Andrographolide (a diterpene lactone from king of bitters, MW 347 Da) is an alicyclic terpenoid built around a bicyclo[3.3.1]decane ring system with three free hydroxyl groups. Its VAL104 hydrophobic contact, at 3.35 Å, is the closest alkyl–alkyl contact recorded in the series. More striking is its interaction with ARG105: andrographolide donates to both the backbone carbonyl and the backbone amide of the same residue, forming a bidirectional H-bond pair (2.66 Å and 3.07 Å) that resembles an anti-parallel β-sheet, an interaction pattern not seen with any other compound. It also forms the conserved GLN110 H-bond (2.63 Å, 124.56°) and a borderline contact with GLN107 (3.43 Å, 102.24°), a residue no other compound in the*

series reaches. Its ligand efficiency (0.240) is comparatively modest, reflecting its higher molecular weight compared with simpler terpenoids.

8) *Quercitrin — ΔG = −5.6 kcal/mol: Quercitrin (quercetin-3-O-α-L-rhamnoside from O. indicum, MW 448 Da) forms only 1 H-bond, with LYS137, but compensates with 3 hydrophobic contacts and a distinctive π-cation interaction with LYS5, a feature unique to this complex in the series. TYR126 contributes an additional hydrophobic contact. The relatively sparse interaction network, and the reliance on a single π-cation interaction rather than a dense H-bond network, is consistent with its comparatively modest docking score.*

9) *Isoquercitrin — ΔG = −5.4 kcal/mol: Isoquercitrin (quercetin-3-O-β-D-glucoside from O. indicum, MW 464 Da) is the only compound in the series that forms no hydrophobic contacts, relying entirely on five H-bonds spread across five distinct residues in a broad region of the binding site. Two of these residues, GLN127 (2.29 Å, the shortest H-bond in this complex) and THR169 (2.49 Å, backbone), do not appear in any other complex, suggesting isoquercitrin reaches a part of the binding site the other compounds do not. Its contacts with GLU288 (104.05°) and GLU290 (115.07°) fall below the 120° angle threshold generally used to define a reliable H-bond, limiting how much they may contribute energetically, while LYS5 provides the strongest electrostatic H-bond in the complex (2.93 Å, 144°).*

10) *6-Gingerol — ΔG = −5.2 kcal/mol: 6-Gingerol (phenylalkanone from ginger, MW 292 Da) is the most conformationally flexible compound tested, with 10 rotatable bonds, and correspondingly has the lowest docking score in the series, a fairly clean illustration of the entropy/enthalpy trade-off in ligand binding. What it lacks in rigidity it partly makes up for with its π-stacking geometry: the vanillyl ring aligns face-to-face with PHE294 in a parallel (P-type) arrangement at 3.76 Å, an angle of 5.45°, and an offset of just 0.44 Å, the most geometrically ideal π-stacking interaction anywhere in the series, estimated to contribute 2–4 kcal/mol to binding. Only one reliable H-bond forms, with GLN110 (2.41 Å, 124.33°); the contacts with SER158 and ASP153 both fall below the 120° angle threshold for reliability. Together, these results point to the vanillyl group as a promising pharmacophore for engaging PHE294, and suggest that shortening the five-carbon alkyl chain could reduce the conformational entropy penalty and improve binding.*

11) *Conserved Residues and General Interaction Patterns: The PLIP analysis across all ten complexes identified several residues that recur consistently, with GLN110 as the most conserved H-bond residue: conserved in 9/10 complexes (absent only in Isoquercitrin). It participates via H-bonding, hydrophobic contact, or both, and exhibits the best H-bond geometry with Artemisinin (168.22°, the closest to ideal in this series).*

• **THR111:** conserved in 4/10 complexes (Quercetin, Baicalein, Naringenin). It serves as a characteristic H-bond hub for small flavone aglycones; Baicalein holds the record of 4 simultaneous H-bonds.

• **PHE294:** the most important aromatic residue in the binding pocket, present in 5/10 complexes in multiple roles — aromatic hydrophobic (Quercetin, Baicalein, Artemisinin, Naringenin) and P-type π-stacking (6-Gingerol, closest at 3.15 Å).

• **VAL104:** forms hydrophobic contacts in 6/10 complexes, notably Andrographolide (3.35 Å, closest alkyl–alkyl contact) and Baicalein (triple contact set 3.62–3.83 Å).

• **LYS5:** present in 6/10 complexes (Oroxin B, Quercetin, Quercitrin, Isoquercitrin, Rutin, Artemisinin) in diverse roles — hydrophobic, H-bond, salt bridge (Oroxin B, Rutin), π-cation (Quercitrin).

• **LYS137:** present in 4/10 complexes (Oroxin B, Quercitrin, Rutin, Baicalein) via H-bonds and salt bridges; Rutin forms the strongest H-bond in the entire series (1.92 Å, 165.92°).

D. Drug-Likeness Assessment

Table IV presents the physicochemical parameters evaluated according to Lipinski and Veber rules, based on SwissADME data.

Table IV. Drug-Likeness Assessment of Ten Compounds (SwissADME Data)

Compound	MW (Da)	LogP	HBD	HBA	TPSA (Å²)	RotB	Viol.	Conclusion
Artemisinin	282.3	3.04	0	5	53.9	1	0	Pass — most optimal
Quercetin	302.2	0.79	5	7	131.4	1	0	Pass — good drug-like
Naringenin	272.3	3.68	2	4	86.9	1	0	Pass — optimal ★
Oroxin B	446.4	−0.67	6	11	187.1	4	2	Fail (HBA, TPSA)
Rutin	610.5	−2.74	10	16	269.4	6	3	Fail — MW, TPSA
Baicalein	270.2	1.53	3	5	90.9	1	0	Pass — optimal ★
Andrographolide	350.4	3.28	3	4	97.9	3	0	Pass — good drug-like

In Silico Screening of 10 Natural Compounds from Oroxylum indicum and Other Medicinal Plants against SARS-CoV-2 Mpro

Compound	MW (Da)	LogP	HBD	HBA	TPSA (Å²)	RotB	Viol.	Conclusion
Quercitrin	448.4	−0.62	7	11	190.3	3	2	Fail (HBD, HBA, TPSA)
Isoquercitrin	464.4	−1.34	8	12	210.5	4	2	Fail (HBD, HBA, TPSA)
6-Gingerol	294.4	4.11	2	4	66.6	10	0	Pass — RotB at Veber limit

HBD: H-bond donors; HBA: H-bond acceptor; RotB: rotatable bond; Viol.: number of Lipinski criteria not satisfied; ★: optimal physicochemical profile.

Figure 4 visualizes the drug-likeness profiles of six representative compounds (Artemisinin, Quercetin, Naringenin, Baicalein, Andrographolide, and 6-Gingerol) as a six-axis radar chart based on Lipinski and Veber rules. A larger shaded area indicates a more favorable drug-likeness profile.

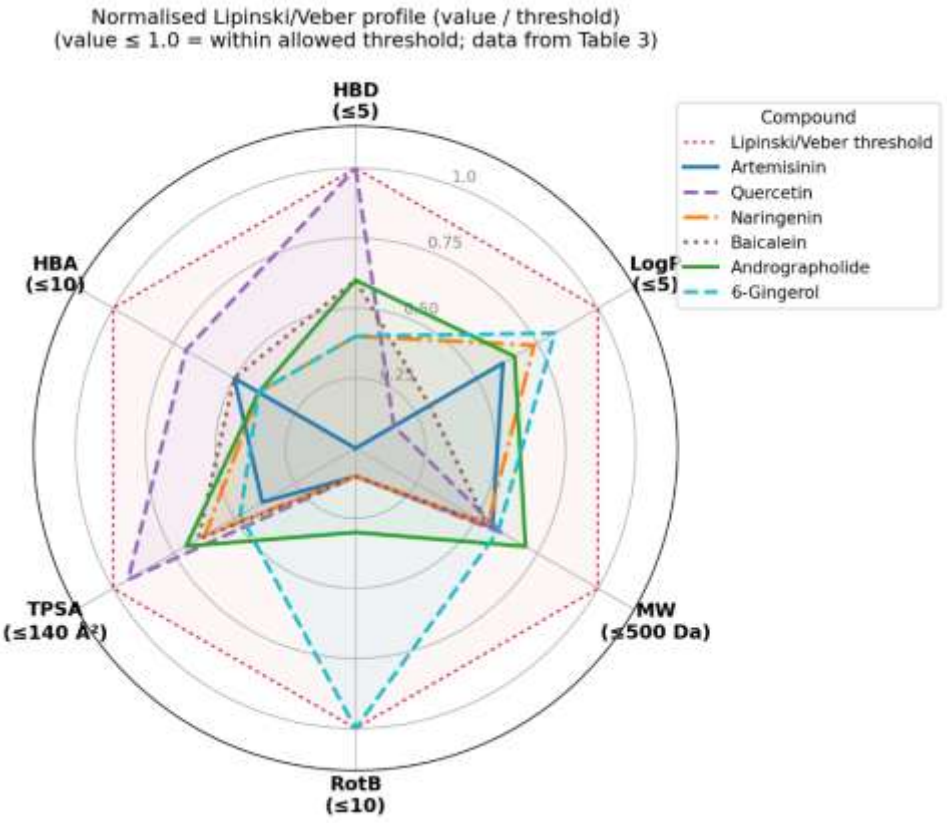

Figure 4. Radar chart comparing drug-likeness profiles of six representative compounds according to Lipinski and Veber rules (normalized values 0–1; 1 = optimal).

Six axes: MW (≤500 Da), LogP (≤5), HBD (≤5), HBA (≤10), TPSA (≤140 Å²), RotB (≤10). Red dashed line: drug-likeness reference threshold. Larger shaded area = better drug-likeness profile. Data from SwissADME (swissadme.ch).

Six of the ten compounds — artemisinin, quercetin, naringenin, baicalein, andrographolide, and 6-gingerol — fully satisfy both Lipinski and Veber criteria. Among them, naringenin and baicalein show the most favorable physicochemical profiles (MW under 270 Da, TPSA under 92 Å², and only 1 rotatable bond), suggesting excellent oral bioavailability and a Bioavailability Score of 0.55 in SwissADME. By contrast, the four glycosides — oroxin B, rutin, quercitrin, and isoquercitrin — violate 2–3 Lipinski criteria because of elevated HBA and TPSA values above 140 Å², although nano-delivery formulations or removal of the glycoside chain could improve this.

E. ADMET Profile

Table V summarises the predicted ADMET pharmacokinetic and safety parameters for the ten compounds, including gastrointestinal absorption (GI absorption), blood–brain barrier permeability (BBB), P-glycoprotein substrate status, PAINS alerts, and Bioavailability Score, as derived from SwissADME and pkCSM.

Table V. Predicted ADMET Pharmacokinetic And Safety Parameters For The Ten Compounds

Compound	GI abs.	BBB	Pgp	PAINS	Bio. Score	Remarks
Artemisinin	High*	Yes*	None	0	0.55*	Extensive malaria clinical record — safest
Quercetin	High	None	None	1	0.55	PAINS alert requires confirmation; high bioavail.
Naringenin	High	None	None	0	0.55	No PAINS; cleanest profile ★
Oroxin B	Low	None	None	1	0.11	Glycoside — nano-formulation required
Rutin	Low	None	None	1	0.17	Nano-delivery clinically established
Baicalein	High	None	None	1	0.55	Anti-SARS-CoV-2 confirmed in vitro [27,28]
Andrographolide	High	Yes*	None	0	0.55	RCT COVID-19 (Thailand) [29]
Quercitrin	Low	None	None	1	0.17	Glycoside — low bioavailability
Isoquercitrin	Low	None	None	1	0.17	Glycoside — special formulation needed
6-Gingerol	High	Yes*	None	0	0.55	GRAS (FDA); high RotB — rapid metabolism

(*) From SwissADME/pkCSM [30] and clinical records. GI abs: gastrointestinal absorption; BBB: blood–brain barrier; Pgp: P-glycoprotein; PAINS: Pan-Assay Interference Compounds; Bio. Score: Bioavailability Score.

Figure 5 shows the relationship between GI absorption and bioavailability score for the ten compounds. Bubble size reflects MW; color distinguishes compounds with and without PAINS alerts; gold stars (★) mark BBB-permeant compounds.

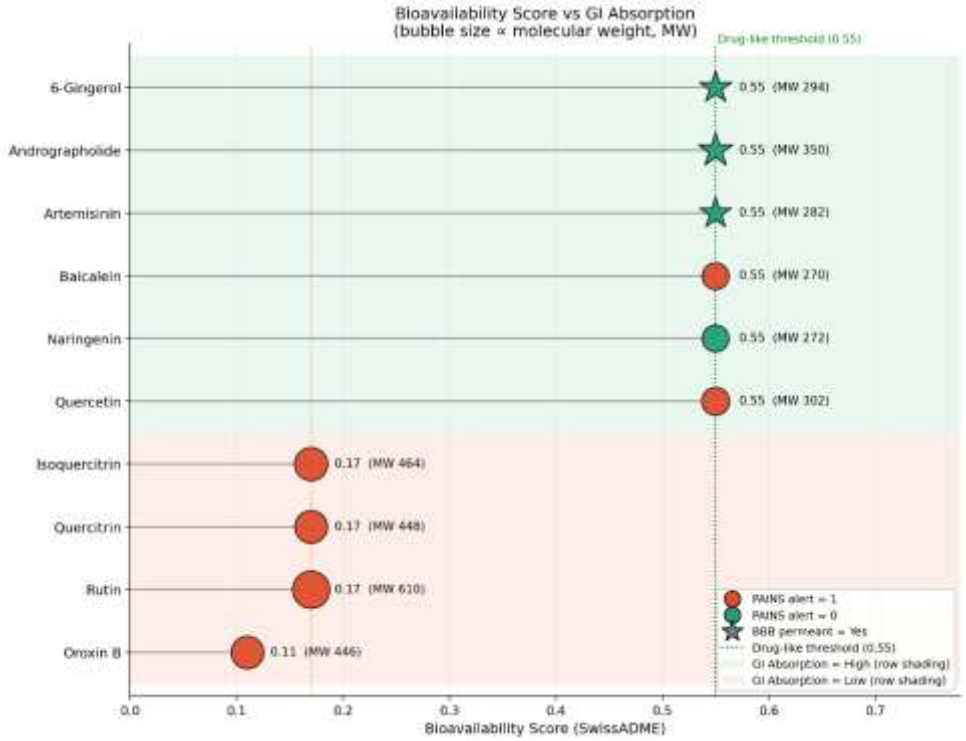

Figure 5. Bubble chart comparing ADMET profiles of ten compounds: GI Absorption vs. bioavailability score (bubble size ∝ MW).

Green with gold star (★): PAINS = 0, BBB permeant = Yes; red-orange: PAINS = 1 (flavonoid alert); plain green: PAINS = 0, BBB = No. Gold star (★): BBB-permeant compound. Data from SwissADME; Bioavailability Score 0.55 = drug-like standard.

1) *Absorption: The small aglycone group, naringenin, baicalein, quercetin, and artemisinin, share a TPSA of 54–131 Å² and 0–1 rotatable bonds, giving all four high predicted GI absorption and a Bioavailability Score of 0.55 in SwissADME. In practice, though, oral bioavailability for several flavonoids runs lower than these in silico predictions suggest, largely because of intestinal and hepatic first-pass metabolism: quercetin reaches only about 1–17% in humans, baicalein around 36% in rats, and artemisinin roughly 30% in humans after a single dose. Naringenin, with the lowest TPSA in the group (86.9 Å²) and no PAINS alerts, has the most favorable predicted absorption and appears to be the strongest candidate for oral development.*

The glycoside group, oroxin B, rutin, quercitrin, and isoquercitrin, fares worse: TPSA of 187–269 Å² and Bioavailability Scores of only 0.11–0.17 predict low GI absorption, which matches what has been observed clinically. This is largely because glycosides need

to be hydrolyzed by β-glucosidase in the intestinal microbiome into their corresponding aglycones (quercetin, baicalein) before they can be absorbed. That extra step brings three practical consequences: considerable inter-individual variability depending on each person's gut microbiome, a delayed Cmax (2–6 h rather than 1–2 h), and generally lower overall bioavailability than the free aglycones achieve. Rutin in particular (TPSA 269 Å², Bioavailability Score 0.17) could benefit from a nanoparticle- or phospholipid-complex formulation, approaches already shown elsewhere to improve bioavailability 5- to 10-fold.

6-Gingerol (10 rotatable bonds, high predicted GI absorption, TPSA 66.6 Å²) is readily absorbed orally but is rapidly broken down, both at the intestinal mucosa and via hepatic first-pass metabolism, into shogaol and zingerone, resulting in a short half-life of around 1–2 h. Andrographolide shows a similar disconnect between prediction and reality: its GI absorption looks favorable on paper (TPSA 97.9 Å²), but actual oral bioavailability is only about 2.7%, limited by poor aqueous solubility and extensive first-pass metabolism. Cyclodextrin complexation or self-emulsifying drug delivery systems are the usual strategies for addressing this limitation.

2) *Distribution:* ***Blood–brain barrier (BBB):*** *Artemisinin, 6-gingerol, and andrographolide are predicted by SwissADME to cross the BBB, a property that could be useful, given that COVID-19 is associated with neuroinflammation and brain fog. Artemisinin's CNS penetration is well established experimentally through its efficacy against cerebral malaria and in neuroinflammation models, and andrographolide has separately shown neuroprotective activity in models of Alzheimer's and Parkinson's disease.*

The remaining seven compounds remain largely in peripheral tissues, which works in their favor for this application: Mpro is targeted in the lungs and respiratory tract, so limited CNS exposure reduces the risk of central side effects. Quercetin and baicalein, despite not crossing the BBB to any meaningful extent, still exert systemic anti-inflammatory effects through NF-κB inhibition and suppression of the cytokine storm, both of which are relevant to severe COVID-19.

P-glycoprotein substrate status and plasma protein binding: None of the ten compounds are predicted by SwissADME to be P-glycoprotein substrates, indicating little risk of active efflux at the intestinal wall, liver, or blood–brain barrier, an advantage over many synthetic antivirals that are strong P-glycoprotein substrates. Regarding plasma protein binding, the polyphenolic flavonoids quercetin and baicalein bind strongly to serum albumin (over 90% in vitro), thereby lowering the free drug concentration but also extending the effective half-life. Artemisinin (logP 3.04) and naringenin (logP 3.68) both strike a reasonable balance between lipophilicity, needed for tissue distribution, and hydrophilicity, needed to stay in circulation.

3) *Metabolism and Drug–Drug Interaction Risk (Metabolism and DDI): CYP450-mediated metabolism is the most critical determinant of drug–drug interaction (DDI) risk and must be evaluated before any combination therapy for COVID-19. The CYP profile of each compound group, based on published in vitro and clinical data, is summarised below:*

• **Quercetin:** inhibits CYP1A2, CYP2C9, CYP2D6, and CYP3A4 moderately to strongly in vitro (Ki <10 μM). Notable interactions include: warfarin (CYP2C9) — elevated INR risk; cyclosporine and statins (CYP3A4) — increased plasma concentrations; and theophylline (CYP1A2). However, owing to its low oral bioavailability (~1–17%), systemic quercetin concentrations are generally insufficient to produce clinically significant CYP inhibition at dietary doses.

• **Baicalein:** clearly inhibits CYP1A2 and CYP2C9; mild CYP3A4 inhibition. Caution is warranted when co-administered with theophylline (CYP1A2), warfarin and phenytoin (CYP2C9).

• **Naringenin:** inhibits CYP1A2 and CYP3A4 via a mechanism analogous to the grapefruit juice effect. At higher concentrations, naringenin can markedly increase the bioavailability of CYP3A4-substrate drugs (statins, immunosuppressants, some antiretrovirals), similarly to grapefruit juice. Patients should be counseled to avoid co-administration.

• **Artemisinin:** CYP3A4 auto-induction — after 5–7 days of continuous use, artemisinin upregulates CYP3A4 via PXR activation, accelerating its own metabolism and causing time-dependent reductions in AUC and Cmax (~50–70% after 7 days of monotherapy). This is the primary rationale for using artemisinin within combination therapy (ACT) rather than as monotherapy. In an anti-COVID-19 context, short-course regimens or co-administration with a CYP3A4 inhibitor would be required to maintain therapeutic concentrations.

• **6-Gingerol:** mild CYP3A4 inhibition, not clinically significant at normal dietary doses (GRAS, FDA). Mild interactions with anticoagulants are possible at high doses, owing to the antiplatelet activity of gingerols.

• **Andrographolide:** moderate CYP3A4 inhibition; caution when co-administered with immunosuppressants. Data from COVID-19 RCTs show that andrographolide 180 mg/day is safe as monotherapy.

• **Glycoside (Oroxin B, Rutin, Quercitrin, Isoquercitrin):** must first be hydrolyzed to their aglycones in vivo before interacting with CYP enzymes; DDI risk therefore arises primarily from released quercetin and baicalein. The magnitude of inhibition is lower than for free aglycones because hydrolysis is incomplete and slow.

Taken together, CYP3A4 is the interaction point that matters most across all ten compounds and warrants close monitoring. Future clinical development should include dedicated DDI studies with co-prescribed CYP3A4 substrates, particularly nirmatrelvir

(Paxlovid, which is itself metabolized via CYP3A4) and remdesivir, as well as any other background medications a COVID-19 patient may be taking.

4) *Excretion: Half-life (T½) and elimination route directly influence dosing schedules. Based on pkCSM predictions and published clinical data:*

• **Artemisinin:** T½ ~1–3 h (shortened by CYP auto-induction); 2–3 doses per day required. Eliminated predominantly via bile as dihydroartemisinin glucuronide.

• **Quercetin and Baicalein:** T½ ~3–5 h; metabolized to glucuronide and sulfate conjugates in the intestine/liver; excreted via kidneys (~30%) and bile (~70%). Conjugates have a longer effective T½ owing to enterohepatic recycling.

• **Naringenin:** T½ ~2–4 h; primarily metabolised by glucuronidation and sulfation; excreted in urine. The glycoside naringin (found in grapefruit) has a longer apparent T½ owing to slower absorption.

• **6-Gingerol:** T½ ~1–2 h; rapidly metabolized in the intestine and liver to shogaol (more bioactive dehydration product) and zingerone; excreted via feces.

• **Andrographolide:** T½ ~0.5–1 h (very short); eliminated mainly via bile as a disulfonate conjugate. Multiple daily doses or a modified-release formulation are required.

• **Glycoside (Oroxin B, Rutin, Quercitrin, Isoquercitrin):** effective T½ depends on the rate of intestinal hydrolysis (2–6 h to reach aglycone Cmax); aglycone conjugates are excreted via the kidneys and bile. Rutin may undergo mild accumulation due to enterohepatic recycling.

5) *Toxicity Prediction: Table VI summarises in silico toxicity predictions (from pkCSM, SwissADME, and published literature) alongside the clinical safety profile of each compound:*

Table VI. Predicted Toxicity and Clinical Safety Profile of the Ten Compounds

Compound	Ames Test	Hepatotox.	hERG	Reproductive Tox.	CYP and Clinical	Conclusion
Artemisinin	Negative	Safe (WHO-approved)	Safe	⚠ Embryotoxic (high doses, animals)	Millions of malaria pts; CYP3A4 auto-inducer	Highly safe
Quercetin	⚠ In vitro positive (in vivo negative)	Safe at food doses	Safe	Safe	GRAS; CYP2C9, CYP1A2 inhibitor — DDI caution	Safe at usual doses
Naringenin	Negative	Safe	Safe	Safe	GRAS; inhibits intestinal CYP3A4 (grapefruit effect)	Safe; monitor CYP3A4 DDI
Oroxin B	⚠ Limited data	Limited data	Limited data	Limited data	Glycoside — limited clinical data	Further studies needed
Rutin	Negative	Safe (supplement)	Safe	Safe	Mild CYP3A4 inhibitor; widely used supplement	Safe
Baicalein	Negative	Hepatoprotective	Safe	Safe	CYP1A2, CYP2C9 inhibitor; anti-SARS-CoV-2 confirmed	Safe; potential anti-COVID high
Andrographolide	Negative	⚠ ALT/AST elevation (high doses, animals)	Safe	⚠ Embryotoxic (high doses, animals)	RCT COVID-19; moderate CYP3A4 inhibitor	Safe at clinical dose; monitor liver
Quercitrin	Negative	Safe	Safe	Safe	Similar to quercetin after hydrolysis	Safe
Isoquercitrin	Negative	Safe	Safe	Safe	Similar to quercetin after hydrolysis	Safe
6-Gingerol	Negative	Safe (GRAS)	Safe	Safe at dietary doses	GRAS FDA; 10 RotB — metabolised rapidly	Highly safe; GRAS FDA

⚠ = caution required; animals = animal studies; pts = patients; DDI = drug–drug interaction; GRAS = Generally Recognized As Safe (FDA); RCT = Randomized Controlled Trial; lit. = from published literature.

PAINS analysis: Six flavonoid compounds, quercetin, baicalein, rutin, quercitrin, isoquercitrin, and oroxin B, each carry one PAINS (Pan-Assay Interference Compounds) alert, tied to the catechol moiety (3',4'-dihydroxy on ring B) or to the flavonoid scaffold generally. A PAINS alert flags a risk of false positives in HTS assays, arising from metal chelation, fluorescence interference, or non-selective covalent reactivity with cysteine or lysine residues on the target protein. That said, a PAINS alert does not mean the biological activity isn't real: quercetin and baicalein have both been confirmed as Mpro inhibitors in vitro by thermal shift assay (DSF) and SPR [27,28], techniques that are not fooled by PAINS-type artifacts. The four PAINS-free compounds in this set, artemisinin, naringenin, 6-gingerol, and andrographolide, should give more straightforward, reliable results in primary HTS screening.

Mutagenicity and genotoxicity: Quercetin tests positive in the Ames assay in certain bacterial systems in vitro, likely because it can form an o-quinone from its catechol group under oxidative conditions, but it is negative in vivo, and both WHO and EFSA consider it safe at normal dietary intake levels. Baicalein, rutin, and naringenin show no meaningful evidence of in vivo mutagenicity, and andrographolide and 6-gingerol are both Ames-negative at pharmacologically relevant concentrations.

Reproductive and developmental toxicity: Artemisinin and andrographolide both show embryotoxicity in animal studies, though only at doses several-fold above the therapeutic range. Artemisinin is classified by the FDA as Pregnancy Category C/D and is not recommended in the first trimester, though it is considered acceptable at standard antimalarial doses in the second and third. Andrographolide has shown antifertility activity in vitro at high doses in some animal models, so caution is warranted in pregnant women, and flavonoids such as quercetin and baicalein have weak phytoestrogenic activity worth considering in patients with hormone-sensitive conditions.

Cardiac toxicity (hERG): None of the ten compounds shows meaningful hERG channel inhibition at pharmacologically relevant concentrations; quercetin (hERG IC_{50} > 30 μM) and baicalein (IC_{50} > 50 μM) both look safe from a cardiotoxicity standpoint, and no clinically significant QT prolongation has been reported for artemisinin at standard doses. That is a meaningful advantage in the COVID-19 setting, where several repurposed drugs, including hydroxychloroquine and azithromycin, are known to prolong the QT interval.

Conclusion: Overall, all ten compounds show an acceptable safety profile at rational therapeutic doses. Artemisinin has by far the most extensive clinical safety record; naringenin and 6-gingerol have the cleanest profiles of the group, with zero PAINS alerts, Ames-negative results, and GRAS status; and andrographolide is the one compound that needs liver function monitoring (ALT/AST) with prolonged use and caution in pregnant women. Across all ten, CYP3A4-mediated drug–drug interactions are the main thing to watch for when co-administering with nirmatrelvir or other CYP3A4-metabolised drugs in a COVID-19 treatment regimen.

IV. DISCUSSION

Taken together, the docking and PLIP results give a fairly complete picture of how these ten compounds engage Mpro. Artemisinin comes out on top by both measures, ΔG (−7.3 kcal/mol) and LE (0.365), and the reason is not hard to see: with zero rotatable bonds, it pays no conformational entropy penalty on binding, so the full enthalpic benefit of its hydrophobic contacts and H-bond shows up directly in the score. The contrast with 6-gingerol, ten rotatable bonds and a score of only −5.2 kcal/mol, makes the same point from the other direction: flexibility carries a real energetic cost.

Across the series, PLIP analysis points to three distinct binding strategies. The first is H-bond-rich: quercetin (10 H-bonds across 6 residues) and baicalein (4 H-bonds with THR111) are small, flat, rigid aglycones that fit the pocket with excellent geometric complementarity. The second is electrostatic: oroxin B and rutin each form 3 salt bridges, with their carboxylate or glucuronate groups engaging LYS5, ARG131, and LYS137. The third relies on hydrophobic and π-interactions: artemisinin (5 hydrophobic contacts) and 6-gingerol (P-type π-stacking with PHE294 at 3.76 Å, 5.45°) both favor these contacts over H-bonding.

Naringenin is arguably the most interesting finding here. It shares a similar hydroxylation pattern with baicalein, an O. indicum compound, yet its non-planar C-ring lets it reach interaction regions the planar flavones cannot, including ARG105 and a PHE294 contact at 3.15 Å, the closest in the series, giving it LE = 0.358, second only to artemisinin. The structure–activity implication is worth flagging: saturating the C-ring of a flavonoid scaffold may improve binding affinity precisely by opening up pockets that planar flavones can't access.

GLN110 appears in 9 of the 10 complexes, making it the most conserved residue in the series and confirming its central role in ligand recognition at Mpro. THR111 serves as the characteristic H-bond hub for the small flavone aglycones (quercetin, baicalein, naringenin), whereas GLU288 and GLU290 show up more often with ligands bearing polar groups, such as oroxin B and isoquercitrin. VAL104 and PHE294 are the conserved hydrophobic anchors, appearing in 6 and 5 complexes, respectively, and PHE294 in particular does double duty, contributing both hydrophobic contacts and π-stacking depending on the ligand.

The ADMET data split fairly cleanly into two groups. The small aglycones, naringenin, baicalein, artemisinin, and quercetin, absorb well orally and share a Bioavailability Score of 0.55, making them the priority candidates for oral development, while the glycosides, oroxin B, rutin, quercitrin, and isoquercitrin, will likely need specialized formulation, nanoparticles, or a phospholipid complex to reach usable bioavailability. Artemisinin is a partial exception even within the first group: its CYP3A4 auto-induction causes concentrations to fall over time, which is why it is normally given as part of combination therapy rather than alone, a liability that naringenin and andrographolide don't share. CYP3A4-mediated drug interactions are a concern for all 10 compounds, especially when coadministered with nirmatrelvir (Paxlovid), which is itself a potent CYP3A4 inhibitor. The seven compounds that don't cross the blood–brain barrier are reasonably well suited to targeting Mpro in the respiratory tract, since limited CNS exposure lowers the risk of central side effects, and the overall toxicity picture is favorable, with andrographolide the only compound that needs hepatic monitoring over extended use.

This work has three main limitations. Static docking cannot capture protein flexibility, so molecular dynamics simulations will be needed to see whether these binding poses actually hold up over time. The in silico ADMET predictions need experimental confirmation. And cell-based SARS-CoV-2 assays, in Vero E6 or Calu-3 cells, remain an essential next step before any of these findings can be taken further. Worth noting: even though 6-gingerol scored lowest of the ten compounds, its π-stacking geometry points to the vanillyl group as a promising pharmacophore for engaging PHE294, suggesting an optimization route that keeps the vanillyl group intact while shortening the alkyl chain to cut rotatable bonds down to three or fewer.

V. CONCLUSIONS

This study evaluated the inhibitory potential of ten natural compounds against SARS-CoV-2 Mpro, six from *Oroxylum indicum* and four from other medicinal plants, using AutoDock Vina molecular docking combined with PLIP v2.4.0 interaction analysis. The key findings are:

(1) Artemisinin (−7.3 kcal/mol, LE 0.365) and naringenin (−6.8 kcal/mol, LE 0.358) achieved the highest ligand efficiency values in the series, reflecting the benefits of molecular rigidity and favorable binding geometry;

(2) Quercetin formed 10 H-bonds, the richest network of any complex, while baicalein combined 4 simultaneous H-bonds with THR111 and 3 hydrophobic contacts with VAL104, making these the two strongest-binding flavone aglycones from O. indicum;

(3) oroxin B and rutin both rely on a salt-bridge strategy through their carboxylate groups, while 6-gingerol forms the most geometrically ideal P-type π-stacking interaction in the series with PHE294 (3.76 Å, 5.45°), pointing to the vanillyl group as a pharmacophore worth pursuing further;

(4) GLN110 (present in 9 of 10 complexes), along with VAL104 and PHE294, emerged as the most consistently important residues and should be a priority in future structure-based drug design;

(5) four compounds, artemisinin, naringenin, baicalein, and quercetin, fully satisfy the Lipinski and Veber criteria, making them the priority candidates for preclinical follow-up.

Together, these results support *Oroxylum indicum*, and baicalein and quercetin in particular, as a promising source of anti-SARS-CoV-2 compounds that merits continued in vitro and in vivo investigation. The priority next steps are molecular dynamics simulations of the top three complexes, Mpro enzyme inhibition assays for baicalein and naringenin, and SAR optimization around the vanillyl pharmacophore of 6-gingerol and the flavanone C-ring scaffold of naringenin.

REFERENCES

1) WHO. COVID-19 Weekly Epidemiological Update, Edition 162. Geneva: WHO; 2023. https://www.who.int/publications/m/item/covid-19-weekly-epidemiological-update (accessed 14 July 2026).
2) Hu B, Guo H, Zhou P, Shi ZL. Characteristics of SARS-CoV-2 and COVID-19. Nat Rev Microbiol. 2021;19(3):141-154. doi:10.1038/s41579-020-00459-7
3) Zhang L, Lin D, Sun X, et al. The crystal structure of the SARS-CoV-2 main protease provides a basis for the design of improved α-ketoamide inhibitors. Science. 2020;368(6489):409-412. doi:10.1126/science. abb3405
4) Anand K, Ziebuhr J, Wadhwani P, Mesters JR, Hilgenfeld R. Coronavirus main proteinase (3CLpro) structure: basis for design of anti-SARS drugs. Science. 2003;300(5626):1763-1767. doi:10.1126/science.1085658
5) Jin Z, Du X, Xu Y, et al. Structure of Mpro from SARS-CoV-2 and discovery of its inhibitors. Nature. 2020;582(7811):289-293. doi:10.1038/s41586-020-2223-y

6) Markov PV, Ghafari M, Beer M, Lythgoe K, Simmonds P, Stilianakis NI, Katzourakis A. The evolution of SARS-CoV-2. Nat Rev Microbiol. 2023;21(6):361-379. doi:10.1038/s41579-023-00878-2
7) Davis HE, McCorkell L, Vogel JM, Topol EJ. Long COVID: major findings, mechanisms and recommendations. Nat Rev Microbiol. 2023;21(3):133-146. doi:10.1038/s41579-022-00846-2
8) Owen DR, Allerton CMN, Anderson AS, et al. An oral SARS-CoV-2 Mpro inhibitor clinical candidate for the treatment of COVID-19. Science. 2021;374(6575):1586-1593. doi:10.1126/science. abl4784
9) Hu Y, Lewandowski EM, Tan H, et al. Naturally occurring mutations of SARS-CoV-2 main protease confer drug resistance to nirmatrelvir. ACS Cent Sci. 2023;9(8):1658-1669. doi:10.1021/acscentsci.3c00538
10) Ullrich S, Nitsche C. The SARS-CoV-2 main protease as drug target. Bioorg Med Chem Lett. 2020;30(17):127377. doi: 10.1016/j.bmcl.2020.127377
11) Newman DJ, Cragg GM. Natural products as sources of new drugs over the nearly four decades from 01/1981 to 09/2019. J Nat Prod. 2020;83(3):770-803. doi: 10.1021/acs.jnatprod.9b01285
12) Atanasov AG, Zotchev SB, Dirsch VM, Supuran CT. Natural products in drug discovery: advances and opportunities. Nat Rev Drug Discov. 2021;20(3):200-216. doi:10.1038/s41573-020-00114-z
13) Mani JS, Johnson JB, Steel JC, Broszczak DA, Neilsen PM, Walsh KB, Naiker M. Natural product-derived phytochemicals as potential agents against coronaviruses: A review. Virus Res. 2020; 284:197989. doi: 10.1016/j.virusres.2020.197989
14) Jagetia GC. A review on the medicinal and pharmacological properties of traditional ethno medicinal plant Sonapatha, Oroxylum indicum. Sinusitis. 2021;5(1):71-89. doi:10.3390/sinusitis5010009
15) Dinda B, Dinda S, DasSharma S, Banik R, Chakraborty A, Dinda M. Therapeutic potentials of baicalin and its aglycone, baicalein, against inflammatory disorders. Eur J Med Chem. 2017; 131:68-80. doi: 10.1016/j.ejmech.2017.03.004
16) Cao R, Hu H, Li Y, et al. Anti-SARS-CoV-2 potential of artemisinins in vitro. ACS Infect Dis. 2020;6(9):2524-2531. doi:10.1021/acsinfecdis.0c00522
17) Tutunchi H, Naeini F, Ostadrahimi A, Hosseinzadeh-Attar MJ. Naringenin, a flavanone with antiviral and anti-inflammatory effects: A promising treatment strategy against COVID-19. Phytother Res. 2020;34(12):3137-3147. doi:10.1002/ptr.6781
18) Haridas M, Sasidhar V, Nath P, Abhithaj J, Sabu A, Rammanohar P. Compounds of Citrus medica and Zingiber officinale for COVID-19 inhibition: in silico evidence for cues from Ayurveda. Futur J Pharm Sci. 2021; 7:13. doi:10.1186/s43094-020-00171-6
19) Sa-ngiamsuntorn K, Suksatu A, Pewkliang Y, et al. Anti-SARS-CoV-2 activity of Andrographis paniculata extract and its major component andrographolide in human lung epithelial cells and cytotoxicity evaluation in major organ cell representatives. J Nat Prod. 2021;84(4):1261-1270. doi: 10.1021/acs.jnatprod.0c01324
20) Kontoyianni M. Docking and virtual screening in drug discovery. Methods Mol Biol. 2017; 1647:255-266. doi:10.1007/978-1-4939-7201-2_18
21) Pinzi L, Rastelli G. Molecular docking: shifting paradigms in drug discovery. Int J Mol Sci. 2019;20(18):4331. doi:10.3390/ijms20184331
22) Salentin S, Schreiber S, Haupt VJ, Adasme MF, Schroeder M. PLIP: fully automated protein-ligand interaction profiler. Nucleic Acids Res. 2015;43(W1): W443-W447. doi:10.1093/nar/gkv315
23) Trott O, Olson AJ. AutoDock Vina: improving the speed and accuracy of docking with a new scoring function, efficient optimization, and multithreading. J Comput Chem. 2010;31(2):455-461. doi:10.1002/jcc.21334
24) Lipinski CA, Lombardo F, Dominy BW, Feeney PJ. Experimental and computational approaches to estimate solubility and permeability in drug discovery and development settings. Adv Drug Deliv Rev. 2001;46(1-3):3-26. doi:10.1016/S0169-409X(00)00129-0
25) Veber DF, Johnson SR, Cheng HY, Smith BR, Ward KW, Kopple KD. Molecular properties that influence the oral bioavailability of drug candidates. J Med Chem. 2002;45(12):2615-2623. doi:10.1021/jm020017n
26) Daina A, Michielin O, Zoete V. SwissADME: a free web tool to evaluate pharmacokinetics, drug-likeness and medicinal chemistry friendliness of small molecules. Sci Rep. 2017; 7:42717. doi:10.1038/srep42717
27) Liu H, Ye F, Sun Q, et al. Scutellaria baicalensis extract and baicalein inhibit replication of SARS-CoV-2 and its 3C-like protease in vitro. J Enzyme Inhib Med Chem. 2021;36(1):497-503. doi:10.1080/14756366.2021.1873977

28) Su HX, Yao S, Zhao WF, et al. Anti-SARS-CoV-2 activities in vitro of Shuanghuanglian preparations and bioactive ingredients. Acta Pharmacol Sin. 2020;41(9):1167-1177. doi:10.1038/s41401-020-0483-6
29) Wanaratna K, Leethong P, Inchai N, Chueawiang W, Sriraksa P, Tabmee A, Sirinavin S. Efficacy and safety of Andrographis paniculata extract in patients with mild COVID-19: a randomized controlled trial. Arch Intern Med Res. 2022;5(3):423-427. doi:10.26502/aimr.0125
30) Pires DEV, Blundell TL, Ascher DB. pkCSM: predicting small-molecule pharmacokinetic and toxicity properties using graph-based signatures. J Med Chem. 2015;58(9):4066-4072. doi:10.1021/acs.jmedchem.5b00104